Adsorption of neutral red and malachite green onto soybean dregs: influencing factors and thermodynamic studies

Wei Li, Shiyao Wang, Lingling Zeng, Xuesong Wang, Zhixin Li, Yanbing Liu, Liya Zhu, Yingjie Dai*

College of Resources and Environment, Northeast Agricultural University, No. 600 Changjiang Road, Xiangfang District, Harbin 150030, China, emails: dai5188@hotmail.com (Y. Dai), weili@neau.edu.cn (W. Li), wsy20021001@163.com (S. Wang), 3202925215@qq.com (L. Zeng), wxsong0117@126.com (X. Wang), 1485975573@qq.com (Z. Li), 2302543981@qq.com (Y. Liu), 3350095189@qq.com (L. Zhu)

ABSTRACT

In this study, sodium dodecyl sulfate (SDS) was used to modify soybean dregs. Modified soybean dregs (MSD) and soybean dregs (SD) were used as adsorbents, and the adsorbents were characterized by the infrared spectrum and pore size analysis. The influencing factors of SD and MSD on the adsorption of neutral red (NR) and malachite green (MG) were studied, and the thermodynamics of the adsorption isotherm and adsorption process were discussed. The findings revealed that the adsorption process was significantly affected by varying pH values and salt ion concentrations within the solution. However, altering the quantity of adsorbent added had no considerable impact on the removal rate of NR. The results of the adsorption isotherm fitting demonstrated that the adsorption process complied with the Langmuir and Temkin isothermal adsorption models. The saturation adsorption amount of NR on SD and MSD are 208 and 227 mg/g, respectively, and that of MG are 41.0 and 125 mg/g, respectively. Moreover, it was observed that the adsorption of NR and MG on SD and MSD followed a spontaneous exothermic pattern, with the SDS-treated MSD adsorbent exhibiting a higher adsorption capacity.

Keywords: Soybean dregs; Adsorption; Malachite green; Neutral red

1. Introduction

With the rapid development of global industrialization, millions of people are trapped in the dilemma of freshwater shortage [1]. If untreated, the discharge of factory wastewater into the environment exacerbates pollution levels, particularly in the case of wastewater originating from printing and dyeing operations. Dyes not only contribute to environmental contamination but also pose health risks to humans, as they have been linked to the onset of various conditions such as allergies, hyperactivity disorders, and cancer [2]. In addition to the environmental contamination caused by dye usage, it is important to note that

contamination of freshwater sources significantly reduces the availability of clean water resources [3]. Not only neutral red (NR) but also malachite green (MG) are common organic dyes. The presence of organic dye pollution in water systems can trigger eutrophication, pose threats to the well-being of aquatic flora and fauna, and even accumulate within the human body, potentially leading to various diseases [4]. NR and MG have diverse applications. NR is known to be cytotoxic and has been extensively studied for its potential adverse effects on various biological systems [5]. Studies have shown that exposure to NR can lead to cellular damage, including DNA fragmentation and oxidative stress [6]. MG is a highly toxic thiazine

* Corresponding author.

dye with significant genotoxicity, as it can induce chromosome breakage [5,7]. Therefore, it poses harmful effects on aquatic organisms and potential risks to human health. Given these circumstances, the development of wastewater treatment technologies is urgently required to mitigate the detrimental consequences associated with dye pollution [8].

Presently, existing methods of wastewater treatment from dyes can be divided into three categories: physical, chemical and biological methods [9]. Attachment, oxidation, biodegradation, ion exchange, flocculation and membrane separation are widely used to clean dye wastewater [10–12]. Nevertheless, these methods often suffer from drawbacks such as lengthy operational periods, high costs, and the generation of toxic by-products, thereby limiting their broader applicability. To overcome these drawbacks, adsorption seems to be a better alternative, cost-effective, easy to operate, efficient and simple to use design, and is considered to be a widely used, environmentally friendly and effective technology [10,13]. Adsorption has proven to be one of the most effective and established methods for treating dye wastewater in the textile industry, being able to transfer some soluble organic dyes from the wastewater to the surface of the adsorbent during the adsorption process [14]. Furthermore, the efficacy of adsorption is heavily influenced by the characteristics of the adsorbent itself, given its solid and highly porous nature [[15–17]]. Therefore, the search for inexpensive and efficient adsorbents for the treatment of dye wastewater is of paramount importance [18].

Biomass such as rice husk [19], grapefruit peel [20], peanut husk [21], sugarcane [22], dewaxed honeycomb [23], algae [24], citrus [9], yellow passion fruit peel [10] and *Eichhornia crassipes* [25] have been widely studied for removing dyes from wastewater. Some functional groups on the surface (e.g., hydroxyl, carboxyl, ether bonds and amino groups) give biomass a natural pore structure, so it is speculated that some biomass has some adsorption potential for pollutants [21,26]. Numerous studies have shown that various biomass materials can be used for the removal of dyes such as NR and MG, for example, rice husk can effectively remove neutral red dye from aqueous solutions after nitric acid treatment, and peanut shells have a maximum adsorption capacity of 37.5 mg/g for NR in aqueous solutions at 22°C [11,27]. Moreover, biomass showed more advantages than other removal methods, and the adsorption capacity for MG was determined to be 38.2 mg/g in a columnar process with Kessiah-based activated carbon [28]. Agricultural wastes, such as defatted soybeans and chicken feathers, have been explored for the removal and recovery of MG from wastewater, showing good feasibility [29,30].

Soybeans are rich in a large number of nutrients usually used in the preparation of food products, such as soy milk and tofu, and a large amount of soybean residue is produced in this process [31,32]. It has been reported that global soybean production yields approximately 20 million tons of soybean dregs annually [33]. Given the rapid deterioration of soybean dregs, inadequate treatment not only results in the wastage of valuable resources but also poses significant environmental challenges [8]. Research has demonstrated that soybean dregs can serve as effective adsorption materials for the removal of water pollutants [34]. Several studies have demonstrated the effective adsorption of dyes from wastewater using de-oiled soybeans as an adsorbent. For example, Gupta et al. [35] used de-oiled soybeans to adsorb carmoisine A dye in water with an adsorption capacity of 5.62×10^{-5} mol/g. Similarly, Mittal et al. [30] utilized de-oiled soybeans as an adsorbent for malachite green dye and observed nearly 100% removal efficiency, particularly at lower concentrations. This finding underscores the favorable adsorption capacity and cost-effectiveness of the agricultural waste material, "de-oiled soybean". Since the surface tension of liquids can be reduced by surfactants, and the presence of surfactants will greatly affect the adsorption of dyes on solid sorbents [36]. Therefore, experts have modified soybean residue on the basis of soybean residue by using sodium dodecyl sulfate (SDS) activated soybean residue for adsorption in aqueous solutions, and it has been found that SDS activated soybean dregs residue enhanced the adsorption of methylene blue in water by the adsorbent [36–38].

Hence, in this study, we used SDS to modify soybean dregs. The adsorption of neutral red and malachite green in an aqueous solution by modified soybean dregs (MSD) and soybean dregs (SD) was studied. Various factors including pH, adsorbent dosage, ionic strength, adsorption kinetics, adsorption isotherm, and thermodynamics were thoroughly investigated. This study mainly aims to explore the influencing factors of SD and MSD adsorption processes and provide a reference for the practical application of this technology.

2. Materials and methods

2.1. Materials and reagents

NR and MG of analytical purity were purchased from Tianjin Fuchen (Tianjin) Chemical Reagent Co., Ltd. SDS was acquired by Sigma Corporation in the USA Sigma. Soybean dregs was collected from the canteen of Northeast Agricultural University. And the soybean dregs was obtained in its raw form without any specific processing or treatment before being used in the study. Concentrated hydrochloric acid, absolute ethanol, and sodium bicarbonate were all analytical grades. Use distilled water.

2.2. Characterization of materials

To perform Fourier-transform infrared spectroscopy (FTIR), a small amount of dried SD and MSD solid powder is mixed with pure potassium bromide solid powder, which is then ground and pressed into flakes. The powders were scanned with a Fourier-transform infrared spectrometer (8400S, M/s Shimadzu Instruments Co., Ltd., Japan) in the wavelength range of 4,000–400 cm^{-1}. The S_{BET} and pore-size distributions of SD and MSD were determined by the S_{BET} and pore size analyzer (3H-2000PM1, M/s Best Instrument Technology Co., Ltd., Beijing, China) for analysis. N$_2$ adsorption was used to measure the S_{BET} and distribution of pore size of SD and MSD. At a relative stress ratio of $P/P_0 = 0.994$, the distribution of pore size was calculated by the Barrett–Joyner–Halenda and Dubinin–Radushkevich methods, and the S_{BET} could be calculated by the Brunauer–Emmett–Teller method [39].

2.3. Preparation of adsorbents

Take a proper amount of fresh soybean dregs, wash them with tap water until the washing liquid is clear, and then rinse them repeatedly with distilled water to remove surface impurities. The washed soybean residue is placed in an electric oven at a constant temperature, dried to a constant weight at 333 K, stored and set aside. Next, the organic solvents ethanol and sodium bicarbonate solution are added to remove the oil from the bean residue, dried to a constant weight and carefully ground. After grinding and passing through a 100 mesh sieve, the SD was obtained and saved for use. When the concentration of SDS is low, it exists as monomers in solution. However, at higher concentrations, monomers aggregate to form micelles, impacting their ion dispersing ability and SDS modification effectiveness. To maximize SDS utility, the concentration at which monomers exhibit the highest degree of ion dispersion in solution, known as the critical micelle concentration (CMC), is selected during the modification process. At the CMC, SDS achieves the highest level of ionization and maximum effectiveness. The CMC of SDS at 25°C is 0.00082 mol/L [40]. Add an appropriate amount of 0.00082 mol/L SDS solution to SD, and stir continuously for 6 h with a magnetic stirrer. Then it was washed repeatedly with distilled water, and it was then dried to a constant weight using electric heating and a constant temperature blower at 333 K. After grinding, the MSD was obtained and stored for l ater use.

2.4. Batch experiments

The adsorption of SD and MSD was investigated through single-factor experiments to examine the impacts of various influencing factors, including pH, adsorbent dosage, and ionic strength. Among them, the adsorbent dosage was 0.4–1.2 g/L, and the concentration of the NaCl solution was 0–0.5 mol/L. Adjust the pH of the dye solution with 0.1 mol/L HCl or 0.1 mol/L NaOH until the pH value is in the range of 2.0–12.0. Set up a group of three parallel experiments and one control experiment. A 25 mL solution of NR or MG at a concentration of 25 mg/L was added to an Erlenmeyer flask containing 50 mL of adsorbent. After sealing, it was placed in a constant temperature oscillation box and oscillated for 2 h at a temperature of 298 K and a rotation speed of 165 rpm. Next, the solution was filtered through a 0.45 mm membrane, the supernatant was taken after centrifugation, and NR and MG absorbance were measured at 540 and 616 nm using a UV-Vis spectrophotometer. The NR-specific concentration and MG-specific concentration in the solution were calculated using the standard curve. The models used in this paper and their corresponding equations are shown in Table 1.

2.5. Desorption and regeneration experiments

Five portions of the adsorbent, accurately weighed at 1.00 g each, were used for the adsorption of dyes. To each 50 mL conical flask, 25 mL of 25 mg/L NR and MG solutions were added along with 1.00 g of the adsorbent. The flasks were sealed with a sealing film and placed in a thermostatic shaker at 25°C and 165 rpm for 2 h. After complete adsorption, the adsorbent was separated and washed repeatedly with distilled water, then dried for further use. Subsequently, the adsorbent was placed in a sealed glass container containing 100 mL of distilled water as the regeneration solution. Next, all glass containers were placed in an ultrasonic bath filled with water and oscillated for 2 h. Finally, the adsorbent was collected after oscillation, washed repeatedly with distilled water, and dried for subsequent adsorption–desorption experiments. This experiment was repeated four times. The removal efficiency and adsorption capacity of NR and MG in each experiment were used as indicators to evaluate the adsorbent's regeneration capability.

3. Results and discussion

3.1. Characteristics of SD and MSD

The identification of characteristic functional groups in the adsorbent can be accomplished through FTIR spectroscopy. In addition, by comparing the infrared spectroscopic results of pre-adsorption and post-adsorption materials, it is possible to qualitatively analyze which functional groups have an important influence. The FTIR of adsorbent SD and adsorbent MSD are shown in Fig. 1. At 3,434.77 and 2,926.21 cm^{-1}, SD is the stretching vibration of hydroxyl (O–H) and alkane (C–H), and at 1,053.92 cm^{-1}, SD is the characteristic peak of ether bond (C–O–C). These functional groups, being characteristic components of cellulose, serve as further confirmation of the cellulose composition in the SD and MSD adsorbents. The stretching vibrations of carbonyl groups (C=O) in aldehydes and ketones were observed at 1,654.72 cm^{-1}. Notably, changes in the peaks of certain chemical bonds were observed, accompanied by a "red-shift" phenomenon resulting from the overlapping of absorption peaks related to the stretching vibrations of specific chemical bonds following the adsorption process for NR and MG. At the same time, the sharpness of the absorption peaks of some functional groups was also weakened to some extent, indicating that these functional groups were involved in the actual adsorption process. In this process, the most obvious changes in the absorption peaks are hydroxyl (O–H), carbonyl (C=O) and ether bonds (C–O–C). Consequently, these three functional groups may be the most important functional groups in the adsorption process for NR and MG.

In addition, the S_{BET} and pore size distribution of the adsorbent were studied. Generally, a higher S_{BET} indicates the presence of a greater number of pore structures. Based on this factor, more adsorption sites make the adsorption of dyes easier. The adsorption–desorption isotherms of SD and MSD were in accordance with the type III adsorption isotherm. The adsorption reaches equilibrium when $P/P_0 = 1$. Based on pore size classification by the International Union of Pure and Applied Chemistry (IUPAC), pores are categorized as micropores ($d < 2$ nm), mesopores (2 nm $< d <$ 50 nm), and macropores ($d > 50$ nm). Notably, the predominant pore structure in the adsorbents is represented by mesopores. The average pore size D of SD and MSD is 12.9 and 13.1 nm, respectively.

Table 1
Kinetic and isothermal models used, as well as thermodynamic analysis

	Equations	References
Kinetic models		
Intraparticle diffusion	$q_t = k_{\text{diff}} t^{0.5} + C$	[41]
Liquid film diffusion	$\ln\left(1 - \dfrac{q_t}{q_e}\right) = -k_{\text{fd}} t$	[42]
Isotherm models		
Langmuir	$\dfrac{1}{q_e} = \dfrac{1}{q_m} + \dfrac{1}{K_L q_m C_e}$ $R_L = \dfrac{1}{1 + K_L C_0}$	[43]
Temkin	$q_e = \alpha \ln K_T + \alpha \ln C_e$	
Thermodynamic analysis		
Van't Hoff formula	$\Delta G^\circ = -RT \ln K_d$ $\ln K_d = \dfrac{\Delta S^\circ}{R} - \dfrac{\Delta H^\circ}{RT}$	[44]
Adsorption model		
Monolayer adsorption model	$Q_e = \dfrac{n D_m}{1 + \left(c_{1/2}/c\right)^n}$	[45]
Bilayer adsorption model	$Q_e = n D_m \dfrac{\left(c/c_1\right)^n + 2\left(c/c_2\right)^{2n}}{1 + \left(c/c_1\right)^n + \left(c/c_2\right)^{2n}}$	[46]

Notes: q_e = adsorption amount at equilibrium; q_t = adsorption amount at time t; C_e is the equilibrium concentration (mg/L) of the dye solution, K_L is the Langmuir equilibrium constant (L/mg), K_T and α are Temkin constants, the value of K_T is related to the adsorption strength, ΔS°, ΔH° and ΔG° are entropy change (J/mol·K), enthalpy change (J/mol) and Gibbs free energy change (J/mol), T is thermodynamic temperature (K) and R is ideal gas constant (8.314 J/mol·K), n is defined as the number of dye molecules (NR or MG) adsorbed per adsorption site (SD or MSD), D_m represents the density of adsorption receptor sites on the material, and $C_{1/2}$ (mg/L) is the half-saturation concentration of cambium. In this model, the saturation adsorption capacity is given by $Q_{esat} = n \cdot D_m$, c_1 and c_2 are defined as the half-saturated concentration associated with the two adsorption layers mentioned.

3.2. Effect of pH

Fig. 2 shows the change in the adsorption effect for different solutions at pH. Since NR converts to precipitation under alkaline conditions [47–49], pH is set to 2.0, 3.0, 4.0, 5.0, and 6.0 in this experiment to explore the effect of NR solution pH on adsorption. At a solution pH of 6.0, the removal rates of NR for SD and MSD reached 95.8% and 96.9%, respectively. According to Fig. 2, the pH value of the solution has an important impact on the adsorption effect. Acidic conditions result in the presence of a substantial quantity of H⁺ ions, which hinder the dissociation of certain hydrocarbons and capacitive groups, thereby weakening the corresponding electrostatic attraction in the solution and diminishing the adsorption capacity. Conversely, an incremental increase in pH promotes polarization ionization and shifts the reaction towards enhanced adsorption [50,51].

For MG, increasing the pH in the conversion solution from 2.0 to 12.0 led to a rapid increase in the removal rate, indicating that the magnitude of the pH affected the adsorption effect. In the experimentally set solution pH range, the removal of both SD and MSD increased, with SD gradually increasing from 24.8% to 94.4% and MSD from 30.4% to 95.1%. According to Fig. 2, it can be divided into two phases. In the first stage, when the pH value is between 2.0 and 8.0, the concentration of H⁺ in the solution shows a downward trend, and cations as chromophores of MG dye molecules are involved in the competition for H⁺ adsorption sites in the solution [52,53]. Hence, the electrostatic attraction enhances the adsorption of the adsorbent with the slight decrease of H⁺ concentration. However, in the second stage, when the pH value is between 8.0 and 12.0, the removal rate gradually decreases. It is mainly because the free molecules of MG in the solution and the molecules of
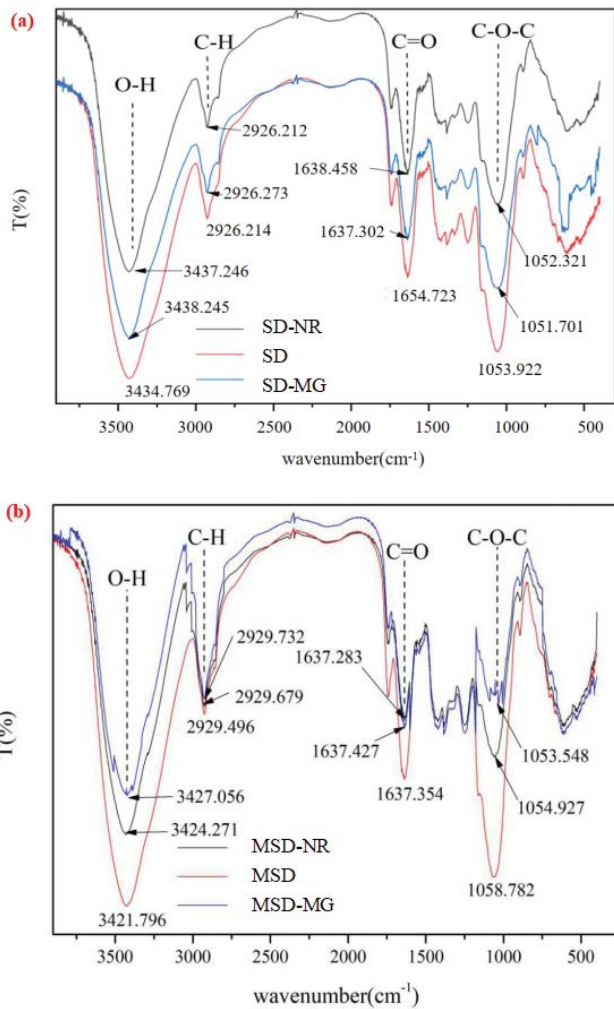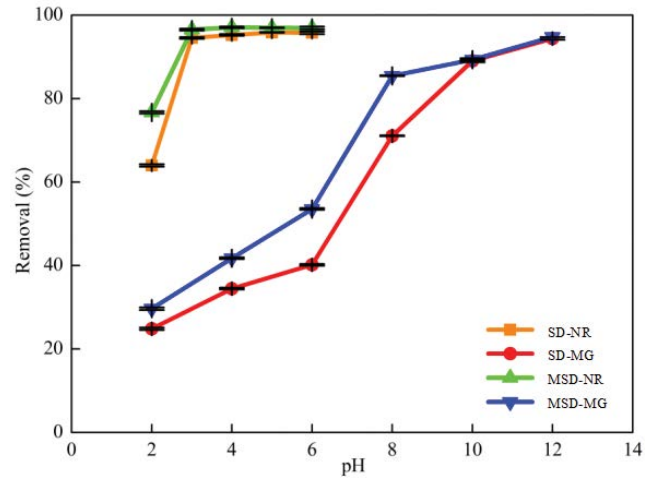
Fig. 2. Effect of solution pH on the adsorption of MG and NR by SD and MSD (concentration of 25 mg/L, temperature 298 K, 120 min equilibrium time).

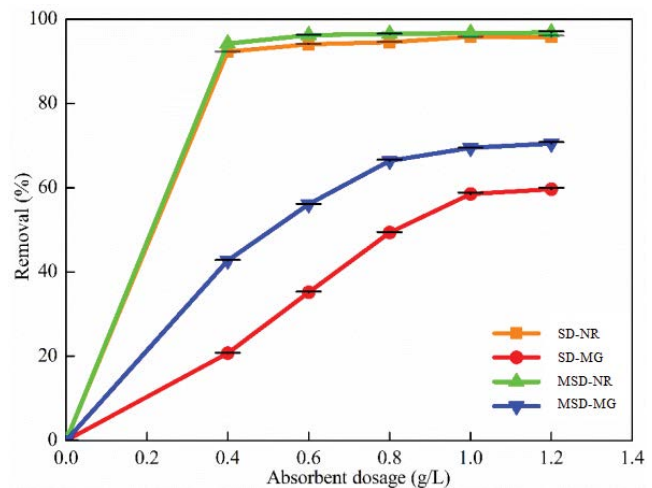Fig. 1. Fourier-transform infrared spectra obtained for (a) SD and (b) MSD.

Fig. 3. Effect of dosage of SD and MSD on the adsorption of MG and NR (concentration of 25 mg/L, temperature 298 K and the equilibrium time of 120 min).

MG adsorbed undergo a displacement reaction. It partially "neutralizes" the electrostatic attraction and the absorption rate changes slowly. Hence, a pH of approximately 8.0 is optimal for MG adsorption experiments. These findings align with the infrared spectroscopic characterization discussed earlier, emphasizing the significant influence of electrostatic interactions on dye adsorption experiments.

3.3. Effect of adsorbent dose

The removal of NR and MG gradually increases with increasing dose and finally tends to an equilibrium state. However, it can be seen from Fig. 3 that for SD and MSD, the change of adsorbent addition has little effect on the removal rate of NR, as the corresponding removal rates were 92.3% and 94.2% at the minimum dose, respectively. After reaching a steady state, the removal rates increased to 95.8% and 96.85%, respectively. For MG, the removal rates increased from 20.7% to 59.7% for SD and from 42.8% to 74.5% for MSD. In NR adsorption, the optimum relative adsorption capacities were about 0.4 g/L for SD and MSD and 1.0 g/L for MG. However, to account for the wide

availability, low-cost, and easy accessibility of raw materials, the relative NR amount in this study was increased to 0.8 g/L in the experiment.

From the experimental conditions, the adsorption effect of MSD was better than that of SD. Surface area and effective fraction are usually related to the amount of adsorbent. As the amount of adsorbent is used, the removal rate also increases. This can be attributed to the availability of ample adsorption sites on the adsorbent, resulting in increased contact area with the dye. But, the removal rate will eventually reach the equilibrium state, which is due to the increase in the amount of adsorbent, making the quantity of adsorbent particles increase and the adsorption surface overlap, leading to partial coverage of the adsorption site. In the meantime, the adsorption capacity decreases with an increase in the adsorbent dose [54,55].

3.4. Effect of ionic strength

In practical dyeing processes, a certain amount of salt is present in the solution. Fig. 4 illustrates the influence of different salt ion concentrations on the adsorption performance. Significant fluctuations in adsorption efficiency can
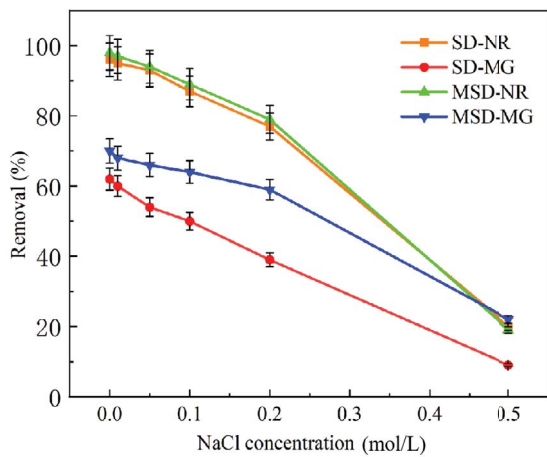

Fig. 4. Effect of ionic strength (concentration of 25 mg/L, temperature 298 K, 120 min equilibrium time).

be observed due to the increasing addition of NaCl. Within the concentration range of 0–0.5 mol/L, the removal efficiency shows a consistent decline, with MSD consistently demonstrating higher removal rates compared to SD. For NR, the removal rates of SD and MSD decrease from the initial values of 94.5% and 96.5% to 20.4% and 20.0%, respectively. For MG, the removal rate of SD decreases from 61.5% to 7.72%, while the removal rate of MSD decreases from 69.3% to 20.5%. The investigation demonstrates the significant influence of salt ion concentration. The introduction of a small quantity of NaCl into the solution initiates a competitive interaction between salt ions and dye molecules for the active sites on the surface of the adsorbent, thereby exerting a pronounced effect on the adsorption performance [56,57].

3.5. Adsorption kinetics

Fig. 5a demonstrates the adsorption rate of the adsorbent is very fast at first and essentially approaches equilibrium in about an hour. In order to know the diffusion mechanism of NR and MG adsorption, we fitted it according to the diffusion equation. The diffusion equations chosen in this experiment are the intraparticle diffusion equation and the liquid film diffusion equation (Table 1). The parameters are shown in Table 2. Fig. 5b and c show that the fitted straight lines of the intraparticle diffusion
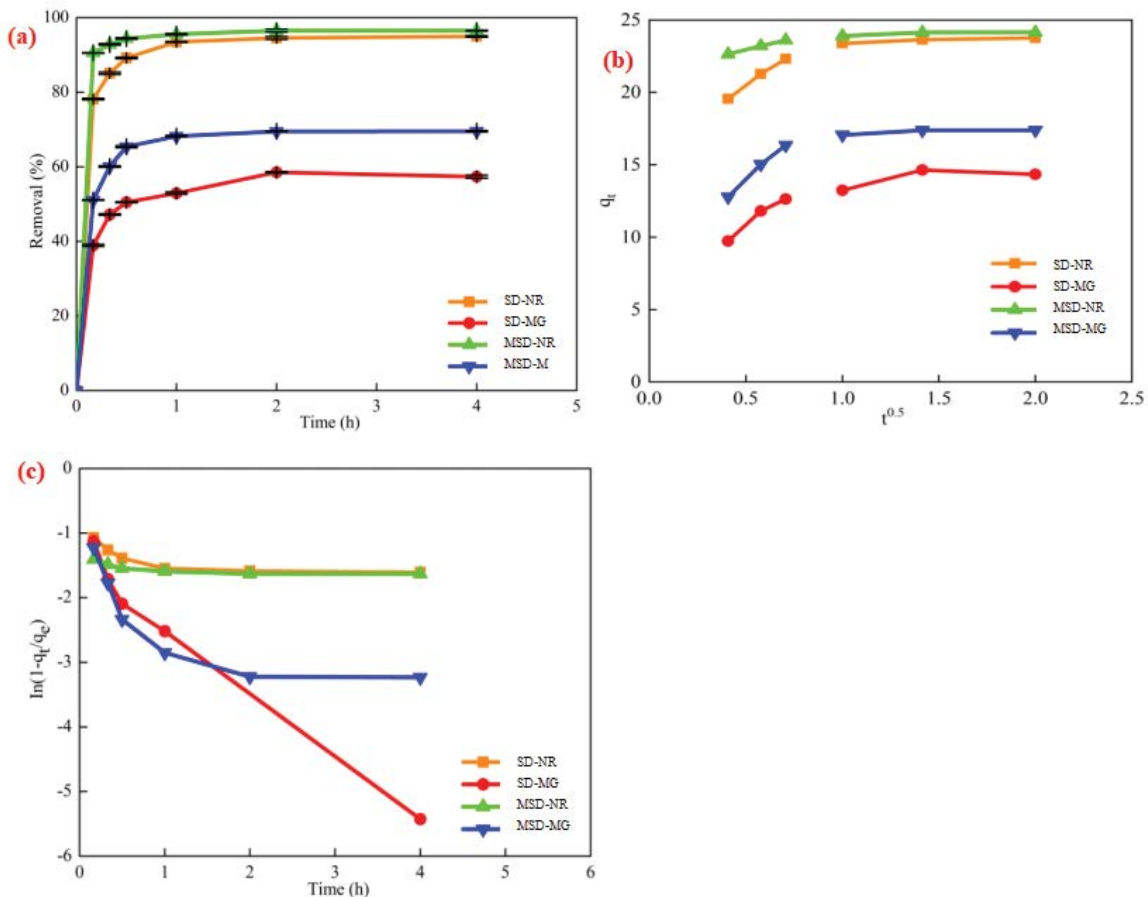

Fig. 5. Adsorption kinetics of SD and MSD (a) time, (b) intraparticle diffusion, and (c) liquid film diffusion.

models for NR and MG do not start from the origin, which indicates that internal diffusion in controlling the adsorption process is not a decisive step [58,59]. Moreover, the inadequacy of the liquid film diffusion model suggests that NR and MG adsorption on the surfaces of SD and MSD is not governed by liquid film coatings.

3.6. Adsorption isotherm

Fig. 6a shows the adsorption isotherms of NR and MG at 298 K, reflecting the relationship between the equilibrium concentration of the solutions and the adsorption amount. It can be obtained from the figure that the equilibrium adsorption amount increases with the concentration of NR and MG solutions and finally stabilizes. This phenomenon can be attributed to the fixed number of available adsorption sites on the adsorbent surface when a constant amount of adsorbent is used. As the solution concentration increases, the adsorption sites on the adsorbent surface become progressively occupied, ultimately resulting in a steady-state adsorption where the amount of adsorbed substance exhibits no significant further change. To further investigate the adsorption model, the Langmuir model and the Temkin model were used (Table 1), which corresponded to the adsorption isotherms, as can be seen in Fig. 6b and c.

From the fitting results of Langmuir isothermal model in Table 3, it can show that R^2 values of NR and MG

adsorbed by SD are 0.967 and 0.965, respectively, and q_m is 208 and 41.0 mg/g, respectively. R^2 values of NR and MG adsorbed by MSD are 0.976 and 0.982, respectively, and q_m is 227 and 125 mg/g, respectively. The value of q_m is similar to the actual measured equilibrium adsorption capacity, so it has been proved that the removal process of NR and MG conforms to Langmuir isothermal model. The results indicate that it is monolayer adsorption, and the adsorbent surface is homogeneous. Moreover, as $R_L < 1.00$, the removal process of these two dyes is very simple [52].

Table 2
Relative parameters table of kinetic models

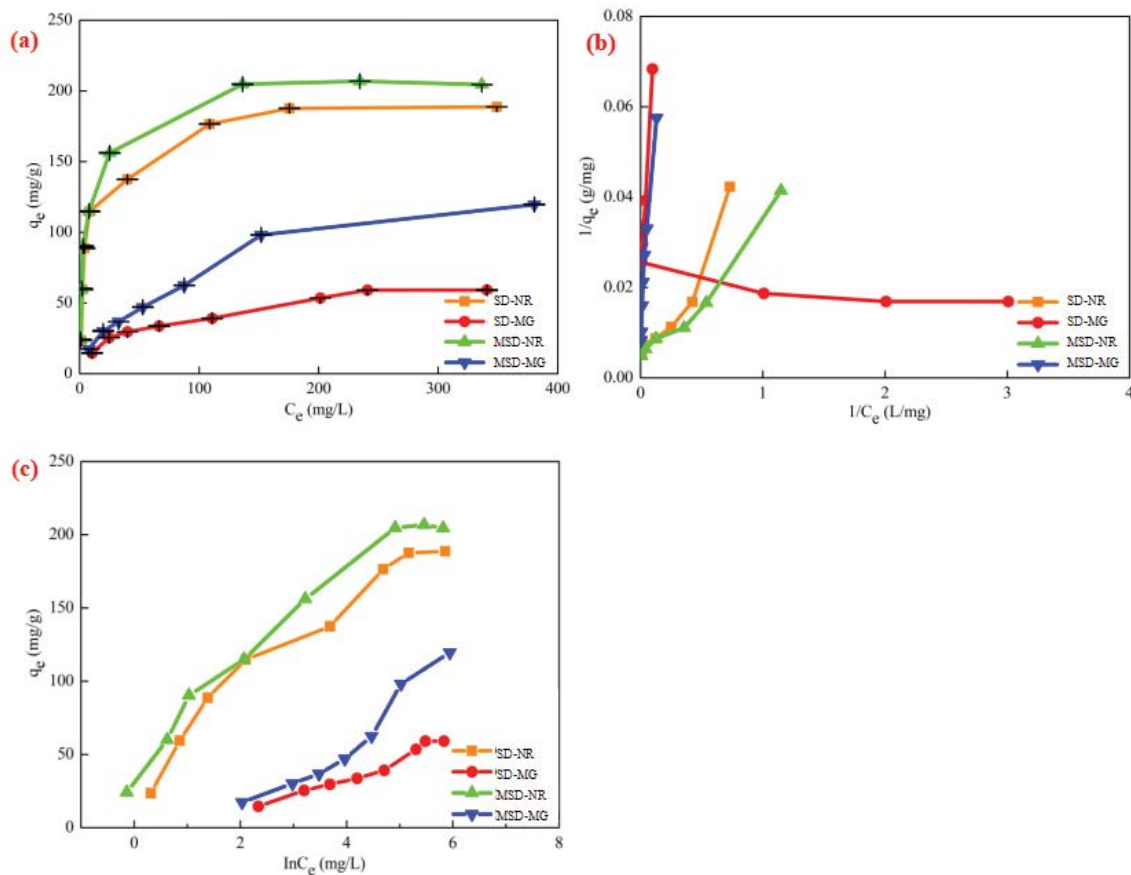| Adsorbent	Models	Parameters	NR	MG
SD	Intraparticle diffusion	k_{id} (mg/g·h$^{1/2}$)	1.02	0.383
		c (mg/g)	21.7	9.13
		R^2	0.932	0.858
	Liquid film diffusion	k_{fd} (h^{-1})	0.108	0.827
		R^2	0.556	0.438
MSD	Intraparticle diffusion	k_{id} (mg/g·h$^{1/2}$)	1.02	0.351
		c (mg/g)	27.4	13.2
		R^2	0.908	0.739
	Liquid film diffusion	k_{fd} (h^{-1})	0.046	0.436
		R^2	0.570	0.609

Fig. 6. Adsorption isotherm of SD and MSD (a) initial concentration of dye, (b) Langmuir, and (c) Temkin.

At the same time, the Temkin model shows the degree of influence of temperature on the adsorption process. For NR, the R^2 values of SD and MSD are 0.967 and 0.956, respectively, revealing that the model has strong applicability and the temperature has a certain influence on the adsorption process [60,61]. For the process of MG adsorption by SD and MSD, the R^2 values fitted by the Temkin isothermal model are 0.975 and 0.993, respectively, indicating that the model fits well and the temperature is closely related to the thermal changes during the adsorption process [62,63].

3.7. Thermodynamics research

In this experiment, the thermodynamic temperatures of the reaction were set to 295, 298 and 304 K. A curve was plotted and linearly fitted using q_e as the independent variable and $\ln(q_e/C_e)$ as the dependent variable. The intercept of the linear regression equation represents the value of K_d [64,65]. Table 1 shows the thermodynamic parameters $\Delta S°$, $\Delta H°$ and $\Delta G°$ were calculated according to the van't Hoff equation. Table 4 indicates the specific thermodynamic parameters. The dispersion coefficients of adsorption, $\Delta S°$, $\Delta H°$ and $\Delta G°$ were changes in entropy (J/mol·K), heat content change (J/mol), and Gibbs function change (J/mol), respectively. T (K) is the thermodynamic temperature and the optimal gas constant is R (8.314 J/mol·K).

It has been proved from the data in Table 4, for NR, the value of $\Delta G°$ is always negative, showing that the adsorption of NR is spontaneous, which reflects the preferential

nature of adsorption. From 295 to 304 K, the $\Delta G°$ values were –2.67, –2.24 and –1.93 kJ/mol for SD and –2.54, –2.23 and –1.90 kJ/mol for MSD. The trend of the $\Delta G°$ values shows that as the temperature increases, the SD and MSD. The $\Delta G°$ values increase, which indicates that the increase in temperature reduces the spontaneity of the reaction, which is exothermic. The $\Delta H°$ value for SD is –26.6 kJ/mol and for MSD is –26.2 kJ/mol. Based on the $\Delta H°$ values, it can be further concluded that the process of NR adsorption by SD and MSD is exothermic.

From the data in Table 4, it can be known that for the $\Delta G°$ of MG is always negative at a diverse range of temperatures, revealing that the adsorption process of MG is carried out spontaneously. When the temperature increased from the initial 298 to 394 K, the values of $\Delta G°$ were –0.900, –0.360 and –0.350 kJ/mol for SD, respectively, and –1.93, –1.39 and –1.27 kJ/mol for MSD, respectively. This indicates that with the increase in temperature, the spontaneity of the reaction becomes smaller, that is, the reaction of SD and MSD adsorption of MG is an exothermic reaction. Meanwhile, the $\Delta H°$ values of SD and MSD were –2.02 and –2.79 kJ/mol, respectively. These two negative values further prove that the reactions of SD and MSD adsorption of MG are exothermic. The values of $\Delta S°$, $\Delta H°$, and $\Delta G°$ for SD are close to zero, indicating that the heat change associated with SD adsorbing MG is extremely small. Also, it is a side indicates that the adsorption of MG by SD is very poor, which echoes the results of the adsorption isotherm model fitted [66,67].

Table 3
Relative parameters of each fitting isotherm

Adsorbents	Dyes	Langmuir				Temkin		
		q_m (mg/g)	K_L (L/mg)	R_L	R^2	K_T	A	R^2
SD	NR	208	0.130	0.01–0.24	0.967	3.35	28.2	0.967
	MG	41.0	0.090	0.03–0.59	0.966	0.68	9.35	0.975
MSD	NR	227	0.170	0.01–0.19	0.976	17.5	23.7	0.956
	MG	125	0.020	0.09–0.71	0.982	0.140	31.4	0.993

Table 4
Related parameters table of thermodynamics

Dyes	Adsorbents	T (K)	K_d	$\Delta H°$ (kJ/mol)	$\Delta S°$ (J/mol·K)	$\Delta G°$ (kJ/mol)
NR	SD	295	2.97			–2.67
		298	2.45	–26.6	79.6	–2.24
		304	2.14			–1.93
	MSD	295	2.81			–2.54
		298	2.52	–26.2	82.0	–2.23
		304	2.12			–1.90
MG	SD	295	1.45			–0.900
		298	1.16	–2.02	–6.52	–0.360
		304	1.15			–0.350
	MSD	295	2.18			–1.93
		298	1.77	–2.79	–8.71	–1.39
		304	1.66			–1.27

Fitting the adsorption data of both dyes with the physical model described can further explain and verify the conclusions obtained in the isotherm and thermodynamic studies. The fit allowed obtaining estimates of the parameters n, D_m and R^2. The results of the fits are shown in Table 5. For NR and MG, the R^2 values for the monolayer adsorption model ranged from 0.938 to 0.996. The R^2 values for the two-layer model were generally very low, ranging from 0.713–0.937. Consequently, the monolayer adsorption model exhibited better fit, indicating that both dyes were adsorbed as monolayers. This finding is in agreement with the conclusion obtained from the Langmuir model fit described. This shows that during adsorption, only the functional groups on the adsorbent and the dye interact [68].

Observing the fitted data in Table 5, by comparing them vertically, it can be found that the q_m of SD and MSD on NR and MG drops as the temperature rises, showing that these adsorption reactions are exothermic. By the cross-sectional comparison, it can be concluded that the adsorption

Table 5
Estimated values of single layer adsorption of the adsorption of MG and NR on SD and MSD

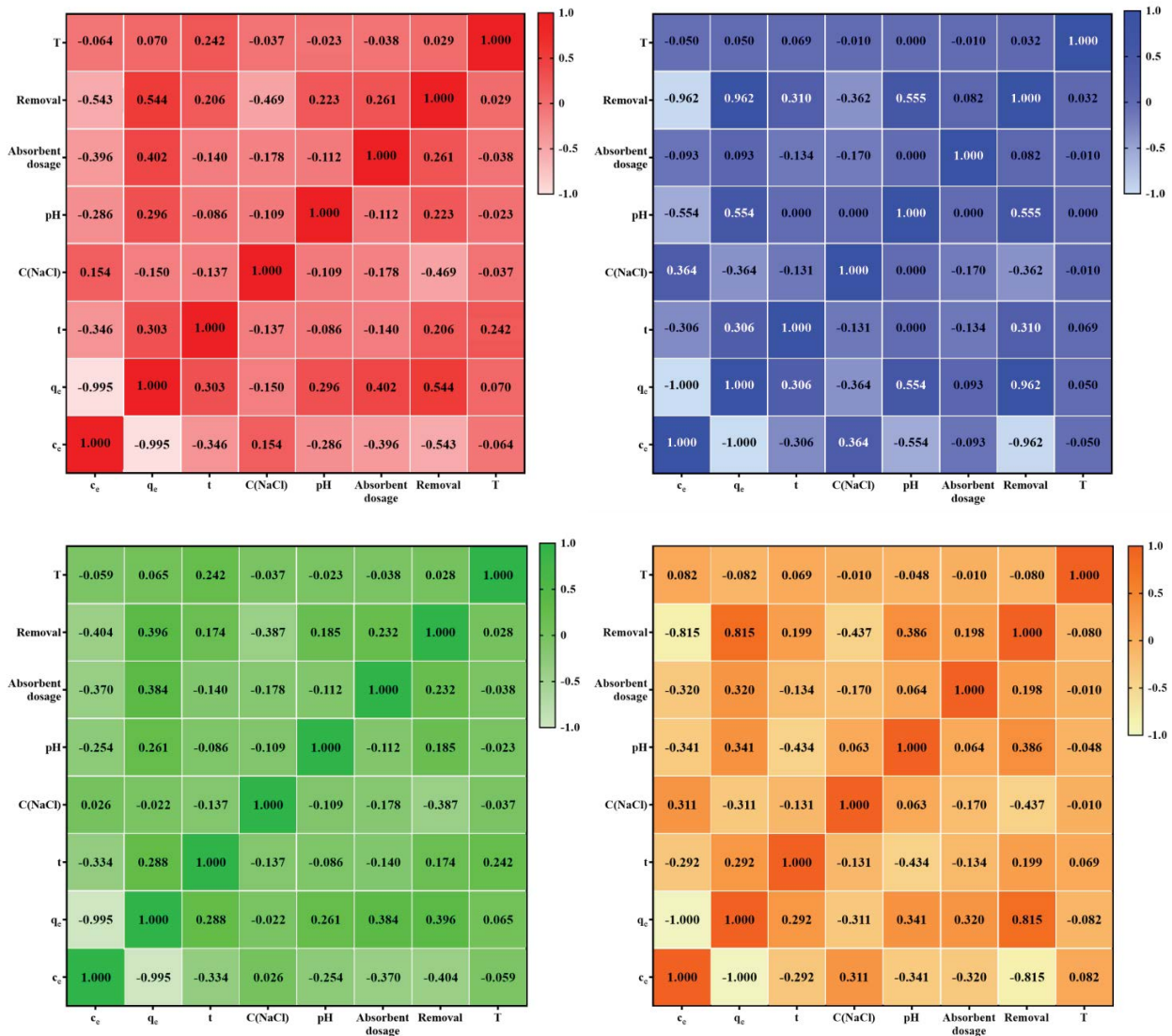|	SD-MG			MSD-MG		
T (K)	295	298	304	295	298	304
n	0.790	0.80	0.75	0.94	1.27	0.88
D_m (mg/g)	94.6	86.4	88.4	174	100	91.9
Q_{esat} (mg/g)	74.7	69.1	66.3	164	127	80.9
R^2	0.996	0.973	0.938	0.988	0.945	0.964
	SD-NR			MSD-NR		
T (K)	295	298	304	295	298	304
n	0.76	0.98	1.51	0.66	0.92	1.22
D_m (mg/g)	268	185	113	383	222	149
Q_{esat} (mg/g)	204	181	171	253	204	182
R^2	0.943	0.954	0.983	0.975	0.982	0.979

Fig. 7. Pearson correlation matrix between any two variables and adsorption efficiency.

Table 6
Pearson correlation coefficient and the corresponding significant level

		T	Removal	Absorbent dosage	pH	C(NaCl)	t	q_e	C_e
					SD-NR				
T	r	1	0.029	–0.038	–0.023	–0.037	0.242	0.07	–0.064
	p		0.889	0.856	0.911	0.859	0.233	0.733	0.757
Removal	r	0.029	1	0.261	0.223	–0.469*	0.206	0.544**	–0.543**
	p	0.889		0.199	0.275	0.016	0.312	0.004	0.004
Adsorbent	r	–0.038	0.261	1	–0.112	–0.178	–0.14	0.402*	–0.396*
dosage	p	0.856	0.199		0.587	0.385	0.495	0.042	0.045
pH	r	–0.023	0.223	–0.112	1	–0.109	–0.086	0.296	–0.286
	p	0.911	0.275	0.587		0.596	0.676	0.142	0.157
C(NaCl)	r	–0.037	–0.469*	–0.178	–0.109	1	–0.137	–0.15	0.154
	p	0.859	0.016	0.385	0.596		0.505	0.464	0.451
t	r	0.242	0.206	–0.14	–0.086	–0.137	1	0.303	–0.346
	p	0.233	0.312	0.495	0.676	0.505		0.133	0.084
q_e	r	0.07	0.544**	0.402*	0.296	–0.15	0.303	1	–0.995**
	p	0.733	0.004	0.042	0.142	0.464	0.133		0
c_e	r	–0.064	–0.543**	–0.396*	–0.286	0.154	–0.346	–0.995**	1
	p	0.757	0.004	0.045	0.157	0.451	0.084	0	
					SD-MG				
T	r	1	0.032	–0.01	0	–0.01	0.069	0.05	–0.05
	p		0.876	0.959	1	0.96	0.731	0.805	0.805
Removal	r	0.032	1	0.082	0.555**	–0.362	0.31	0.962**	–0.962**
	p	0.876		0.684	0.003	0.063	0.115	0	0
Adsorbent	r	–0.01	0.082	1	0	–0.17	–0.134	0.093	–0.093
dosage	p	0.959	0.684		1	0.397	0.505	0.644	0.644
pH	r	0	0.555**	0	1	0	0	0.554**	–0.554**
	p	1	0.003	1		1	1	0.003	0.003
C(NaCl)	r	–0.01	–0.362	–0.17	0	1	–0.131	–0.364	0.364
	p	0.96	0.063	0.397	1		0.514	0.062	0.062
t	r	0.069	0.31	–0.134	0	–0.131	1	0.306	–0.306
	p	0.731	0.115	0.505	1	0.514		0.121	0.121
q_e	r	0.05	0.962**	0.093	0.554**	–0.364	0.306	1	–1.00**
	p	0.805	0	0.644	0.003	0.062	0.121		0
c_e	r	–0.05	–0.962**	–0.093	–0.554**	0.364	–0.306	–1.00**	1
	p	0.805	0	0.644	0.003	0.062	0.121	0	
					MSD-NR				
T	r	1	0.028	–0.038	–0.023	–0.037	0.242	0.065	–0.059
	p		0.891	0.856	0.911	0.859	0.233	0.753	0.776
Removal	r	0.028	1	0.232	0.185	–0.387	0.174	0.396*	–0.404*
	p	0.891		0.254	0.364	0.051	0.396	0.045	0.041
Adsorbent	r	–0.038	0.232	1	–0.112	–0.178	–0.14	0.384	–0.37
dosage	p	0.856	0.254		0.587	0.385	0.495	0.053	0.063
pH	r	–0.023	0.185	–0.112	1	–0.109	–0.086	0.261	–0.254
	p	0.911	0.364	0.587		0.596	0.676	0.197	0.211
C(NaCl)	r	–0.037	–0.387	–0.178	–0.109	1	–0.137	–0.022	0.026
	p	0.859	0.051	0.385	0.596		0.505	0.916	0.899
t	r	0.242	0.174	–0.14	–0.086	–0.137	1	0.288	–0.334
	p	0.233	0.396	0.495	0.676	0.505		0.153	0.096
q_e	r	0.065	0.396*	0.384	0.261	–0.022	0.288	1	–0.995**
	p	0.753	0.045	0.053	0.197	0.916	0.153		0
c_e	r	–0.059	–0.404*	–0.37	–0.254	0.026	–0.334	–0.995**	1
	p	0.776	0.041	0.063	0.211	0.899	0.096	0	

Table 6 (Continued)

Table 6

		T	Removal	Absorbent dosage	pH	$C(NaCl)$	t	q_e	C_e
				MSD-MG					
T	r	1	–0.08	–0.01	–0.048	–0.01	0.069	–0.082	0.082
	p		0.693	0.959	0.814	0.96	0.731	0.685	0.685
Removal	r	–0.08	1	0.198	0.386*	–0.437*	0.199	0.815**	–0.815**
	p	0.693		0.322	0.047	0.023	0.319	0	0
Adsorbent dosage	r	–0.01	0.198	1	0.064	–0.17	–0.134	0.32	–0.32
	p	0.959	0.322		0.75	0.397	0.505	0.104	0.104
pH	r	–0.048	0.386*	0.064	1	0.063	–0.434*	0.341	–0.341
	p	0.814	0.047	0.75		0.755	0.024	0.081	0.081
$C(NaCl)$	r	–0.01	–0.437*	–0.17	0.063	1	–0.131	–0.311	0.311
	p	0.96	0.023	0.397	0.755		0.514	0.114	0.114
t	r	0.069	0.199	–0.134	–0.434*	–0.131	1	0.292	–0.292
	p	0.731	0.319	0.505	0.024	0.514		0.139	0.139
q_e	r	–0.082	0.815**	0.32	0.341	–0.311	0.292	1	–1.00**
	p	0.685	0	0.104	0.081	0.114	0.139		0
c_e	r	0.082	–0.815**	–0.32	–0.341	0.311	–0.292	–1.00**	1
	p	0.685	0	0.104	0.081	0.114	0.139	0	

(**$p < 0.01$; *$p < 0.05$)

capacity of MSD is always greater than that of SD for both adsorptions on NR and MG. These are in agreement with the results obtained in the thermodynamic study, indicating that the MSD adsorbent obtained by treatment with SDS has a stronger application capability [69].

3.8. Regenerative adsorption experimental analysis

SD and MSD were subjected to five cycles of adsorption–desorption experiments for NR and MG. According to the data, SD exhibited regeneration efficiencies of 94.4%, 85.2%, 80.8%, 74.1%, and 69.7% in the first five cycles for NR. Meanwhile, MSD achieved removal efficiencies of 96.5%, 87.4%, 82.3%, 77.1%, and 71.4% for NR in the same five cycles. As for MG, SD demonstrated a decrease in regeneration efficiency from 59.4% to 37.6% over the first five cycles, while MSD showed a decrease from 72.3% to 51.3% in regeneration efficiency over the same five cycles. Both adsorbents exhibited a significant decrease in regeneration efficiency and adsorption capacity after five cycles of desorption–adsorption, indicating that the structure of SD and MSD was disrupted under the influence of ultrasonic oscillation, thereby affecting the adsorption performance [70].

3.9. Correlation between adsorption effect and influencing factors

To further explore the adsorption process of SD and MSD, partial data of nine relevant factors (including reaction temperature (T), dye molecule removal rate, adsorbent dosage, pH of a solution, ion concentration, initial concentration of dye solution (c_0), reaction time (t), adsorption capacity (q_e), equilibrium concentration (c_e) were selected and Pearson correlation coefficients were obtained using SPSS (Table 6). According to the Pearson correlation matrix, four correlation heat maps can be obtained separately (Fig. 7).

The study and analysis of the coefficients in the four matrices can be obtained as follows: (i) In the adsorption of MG by SD and MSD, respectively, the pH and the removal rate are both significantly and positively correlated at the level of 0.05, indicating that the adsorption process of MG is strongly impacted by the pH of the solution. This shows that the electrostatic attraction of SD and MSD plays a key role in adsorption. (ii) Upon observing the four correlation matrices, it was determined that there was no significant correlation between the adsorbent dosage and the removal rate. This indicates that the adsorbent dosage does not have a substantial impact on the removal rate for either the adsorption of SD or MSD. These results were obtained during the analysis of the effect of the adsorbent dosage. (iii) In the SD-NR matrix, the adsorbent dose and q_e were significantly positively correlated at the 0.05 level, which implies that the adsorbent dose will have a significant effect on its adsorption capacity. Moreover, this positive correlation indicates that the removal efficiency of the adsorbent increases with the amount of adsorbent.

4. Conclusion

In this study, the removal capacity of NR and MG through SD and MSD was discussed. It provided a theoretical basis for the removal of dyes in water. On the whole, the adsorption performance of MSD has been improved compared with SD, which shows that the method of modifying soybean dregs by SDS is feasible. The pH value played a crucial role in determining the adsorption efficiency of the adsorbent. The amount of H^+ in the solution will seriously affect the adsorption effect due to the presence of electrostatic attraction. When the concentration of H^+ decreases gradually, electrostatic attraction is going to be beneficial to the adsorption of the adsorbent. The existence of salt ions

in solution can inhibit dye adsorption because salt ions and dye molecules will compete for active sites on the surface of the adsorbent, which greatly affects the adsorption effect. According to the analysis of adsorption isotherm, the q_m of SD and MSD to NR is 208 and 227 mg/g, respectively, and the q_m of MG is 41.0 and 125 mg/g, respectively. Thermodynamic analysis indicated that the adsorption of SD and MSD onto NR and MG was exothermic, confirming the spontaneity of the adsorption process. The inexpensive and readily available adsorbent raw materials used in this study exhibited excellent adsorption effects, offering practical value for potential applications.

References

[1] H.A. Chanzu, J.M. Onyari, P.M. Shiundu, Brewers' spent grain in adsorption of aqueous Congo red and malachite green dyes: batch and continuous flow systems, J. Hazard. Mater., 380 (2019) 120897, doi: 10.1016/j.jhazmat.2019.120897.

[2] J. Mittal, Permissible synthetic food dyes in India, Resonance, 25 (2020) 567–577.

[3] J. Si, B.-K. Cui, Y. Yuan, Y.-C. Dai, Biosorption performances of raw and chemically modified biomasses from *Perenniporia subacida* for heterocycle dye neutral red, Desal. Water Treat., 57 (2016) 8454–8469.

[4] D. Asma, S. Kahraman, S. Cing, O. Yesilada, Adsorptive removal of textile dyes from aqueous solutions by dead fungal biomass, J. Basic Microbiol., 46 (2006) 3–9.

[5] A. Mariyam, J. Mittal, F. Sakina, R.T. Baker, A.K. Sharma, A. Mittal, Efficient batch and fixed-bed sequestration of a basic dye using a novel variant of ordered mesoporous carbon as adsorbent, Arabian J. Chem., 14 (2021) 103186, doi: 10.1016/j.arabjc.2021.103186.

[6] M. Iram, C. Guo, Y. Guan, A. Ishfaq, H. Liu, Adsorption and magnetic removal of neutral red dye from aqueous solution using Fe_3O_4 hollow nanospheres, J. Hazard. Mater., 181 (2010) 1039–1050.

[7] A. Mohamed, M. Ghobara, M. Abdelmaksoud, G. Mohamed, A novel and highly efficient photocatalytic degradation of malachite green dye via surface modified polyacrylonitrile nanofibers/biogenic silica composite nanofibers, Sep. Purif. Technol., 210 (2019) 935–942.

[8] J.F. Gao, C.Y. Si, Y. He, Application of soybean residue (okara) as a low-cost adsorbent for reactive dye removal from aqueous solution, Desal. Water Treat., 53 (2015) 2266–2277.

[9] M. Asgher, H.N. Bhatti, Evaluation of thermodynamics and effect of chemical treatments on sorption potential of Citrus waste biomass for removal of anionic dyes from aqueous solutions, Ecol. Eng., 38 (2012) 79–85.

[10] H. Lin, K.W. Chen, L.L. Du, P. Gao, J.L. Zheng, Y.L. Liu, L.L. Ma, Efficient and selective adsorption of methylene blue and methyl violet dyes by yellow passion fruit peel, Environ. Technol., 43 (2022) 3519–3530.

[11] V. Ponnusami, V. Krithika, R. Madhuram, S.N. Srivastava, Biosorption of reactive dye using acid-treated rice husk: factorial design analysis, J. Hazard. Mater., 142 (2007) 397–403.

[12] H. Wang, X.Z. Yuan, G.M. Zeng, L.J. Leng, X. Peng, K.L. Liao, L.J. Peng, Z.H. Xiao, Removal of malachite green dye from wastewater by different organic acid-modified natural adsorbent: kinetics, equilibriums, mechanisms, practical application, and disposal of dye-loaded adsorbent, Environ. Sci. Pollut. Res., 21 (2014) 11552–11564.

[13] V. Kumar, P. Saharan, A.K. Sharma, A. Umar, I. Kaushal, A. Mittal, Y. Al-Hadeethi, B. Rashad, Silver doped manganese oxide-carbon nanotube nanocomposite for enhanced dye-sequestration: isotherm studies and RSM modelling approach, Ceram. Int., 46 (2020) 10309–10319.

[14] A. Patel, S. Soni, J. Mittal, A. Mittal, C. Arora, Sequestration of crystal violet from aqueous solution using ash of black turmeric rhizome, Desal. Water Treat., 220 (2021) 342–352.

[15] A. Mariyam, J. Mittal, F. Sakina, R.T. Baker, A.K. Sharma, A. Mittal, Efficient batch and fixed-bed sequestration of a basic dye using a novel variant of ordered mesoporous carbon as adsorbent, Arabian J. Chem., 14 (2021) 103186, doi: 10.1016/j.arabjc.2021.103186.

[16] L.Q. Xie, X.Y. Jiang, J.G. Yu, A novel low-cost bio-sorbent prepared from crisp persimmon peel by low-temperature pyrolysis for adsorption of organic dyes, Molecules, 27 (2022) 5160, doi: 10.3390/molecules27165160.

[17] W.H. Zou, H.J. Bai, K. Li, X.L. Shi, R.P. Han, Use of oxalic acid-modified rice husk for the adsorption of neutral red from aqueous solutions, Adsorpt. Sci. Technol., 28 (2010) 641–656.

[18] W.H. Zou, P. Han, Y.L. Lia, X. Liu, X.T. He, R.P. Han, Equilibrium, kinetic and mechanism study for the adsorption of neutral red onto rice husk, Desal. Water Treat., 12 (2009) 210–218.

[19] Y. Safa, H.N. Bhatti, Adsorptive removal of direct dyes by low-cost rice husk: effect of treatments and modifications, Afr. J. Biotechnol., 10 (2011) 3128–3142.

[20] Y.F. Zhan, L. Yang, J.W. Lan, J.J. Shang, S.Q. Chen, X.M. Guan, W.X. Li, S.J. Lin, Mussel-inspired polydopamine decorated pomelo peel as a durable biosorbent for adsorption of cationic dyes, Cellulose, 28 (2021) 453–470.

[21] S. Sadaf, H.N. Bhatti, Batch and fixed bed column studies for the removal of Indosol Yellow BG dye by peanut husk, J. Taiwan Inst. Chem. Eng., 45 (2014) 541–553.

[22] A. Yadav, N. Bagotia, S. Yadav, N. Sharma, A.K. Sharma, S. Kumar, Environmental application of *Saccharum munja* biomass-derived hybrid composite for the simultaneous removal of cationic and anionic dyes and remediation of dye polluted water: a step towards pilot-scale studies, Colloids Surf., A, 650 (2022) 129539, doi: 10.1016/j.colsurfa.2022.129539.

[23] R. Kumari, M.A. Khan, M. Mahto, M.A. Qaiyum, J. Mohanta, B. Dey, S. Dey, Dewaxed honeycomb as an economic and sustainable scavenger for malachite green from water, ACS Omega, 5 (2020) 19548–19556.

[24] E. Rubin, P. Rodriguez, R. Herrero, M.E.S. Vicente, Adsorption of methylene blue on chemically modified algal biomass: equilibrium, dynamic, and surface data, J. Chem. Eng. Data, 55 (2010) 5707–5714.

[25] E. López-Ahumada, M. Salazar-Hernández, A. Talavera-López, O.J. Solis-Marcial, R. Hernández-Soto, J.P. Ruelas-Leyva, J.A. Hernández, Removal of anionic and cationic dyes present in solution using biomass of *Eichhornia crassipes* as bioadsorbent, Molecules, 27 (2022) 6442, doi: 10.3390/molecules27196442.

[26] Y.F. Zhan, L. Yang, J.W. Lan, J.J. Shang, S.Q. Chen, X.M. Guan, W.X. Li, S.J. Lin, Mussel-inspired polydopamine decorated pomelo peel as a durable biosorbent for adsorption of cationic dyes, Cellulose, 28 (2021) 453–470.

[27] W.H. Zou, H.J. Bai, S.P. Gao, X. Zhao, R.P. Han, Investigations on the batch performance of cationic dyes adsorption by citric acid modified peanut husk, Desal. Water Treat., 49 (2012) 41–56.

[28] C. Arora, P. Kumar, S. Soni, J. Mittal, B. Singh, Efficient removal of malachite green dye from aqueous solution using *Curcuma caesia* based activated carbon, Desal. Water Treat., 195 (2020) 341–352.

[29] A. Mittal, Adsorption kinetics of removal of a toxic dye, malachite green, from wastewater by using hen feathers, J. Hazard. Mater., 133 (2006) 196–202.

[30] A. Mittal, L. Krishnan, V.K. Gupta, Removal and recovery of malachite green from wastewater using an agricultural waste material, de-oiled soya, Sep. Purif. Technol., 43 (2005) 125–133.

[31] T.A.H. Nguyen, H.H. Ngo, W.S. Guo, J.L. Zhou, J. Wang, H. Liang, G. Li, Phosphorus elimination from aqueous solution using 'zirconium loaded okara' as a biosorbent, Bioresour. Technol., 170 (2014) 30–37.

[32] B.Y.Z. Hiew, L.Y. Lee, X.J. Lee, S. Thangalazhy-Gopakumar, S. Gan, Utilisation of environmentally friendly okara-based biosorbent for cadmium(II) removal, Environ. Sci. Pollut. Res., 28 (2021) 40608–40622.

[33] C.L. Yu, B.L. Li, K.X. Zhang, F. Li, H. Yan, Adsorption capacity of sodium dodecyl sulfate activation okara for methylene blue on aqueous solution, Korean J. Chem. Eng., 39 (2022) 198–208.

[34] B. Tang, G.P. Peng, D.Y. Luo, X. Zhou, Preparation and adsorption properties of soybean dreg/hydrocalumite composites, ACS Omega, 6 (2021) 27491–27500.

[35] V.K. Gupta, A. Mittal, A. Malviya, J. Mittal, Adsorption of carmoisine A from wastewater using waste materials—bottom ash and deoiled soya, J. Colloid Interface Sci., 335 (2009) 24–33.

[36] Z. Aksu, S. Ertuğrul, G. Dönmez, Methylene blue biosorption by *Rhizopus arrhizus*: effect of SDS (sodium dodecylsulfate) surfactant on biosorption properties, Chem. Eng. J., 158 (2010) 474–481.

[37] C.L. Yu, B.L. Li, K.X. Zhang, F. Li, H. Yan, Adsorption capacity of sodium dodecyl sulfate activation okara for methylene blue on aqueous solution, Korean J. Chem. Eng., 39 (2022) 198–208.

[38] A. Oraon, A.K. Prajapati, M. Ram, V.K. Saxena, S. Dutta, A.K. Gupta, Synthesis, characterization, and application of microporous biochar prepared from *Pterospermum acerifolium* plant fruit shell waste for methylene blue dye adsorption: the role of surface modification by SDS surfactant, Biomass Convers. Biorefin., 5 (2022) 1–23.

[39] S. Ortiz-Monsalve, M. Gutterres, P. Valente, J. Plácido, S. Bustamante-López, D. Kelly, S.L. Kelly, Degradation of a leather-dye by the combination of depolymerised wood-chip biochar adsorption and solid-state fermentation with *Trametes villosa* SCS-10, Bioresour. Bioprocess., 7 (2020) 61, doi: 10.1186/s40643-020-00349-z.

[40] Y. Wang, B. Zhang, Q.C. Ma, Y. Liu, Preparation of non-conductive samples for field emission scanning electron microscopy, Anal. Instrum., 2 (2018) 164–166.

[41] H.B. Zhang, J.Q. Wang, B.Y. Zhou, Y. Zhou, Z.F. Dai, Q. Zhou, P. Christie, Y.M. Luo, Enhanced adsorption of oxytetracycline to weathered microplastic polystyrene: kinetics, isotherms and influencing factors, Environ. Pollut., 243 (2018) 1550–1557.

[42] H. Qiu, L. Lv, B.C. Pan, Q.J. Zhang, W.M. Zhang, Q.X. Zhang, Critical review in adsorption kinetic models, J. Zhejiang Univ.-Sci. A, 10 (2009) 716–724.

[43] S. Agarwal, P. Rajoria, A. Rani, Adsorption of tannic acid from aqueous solution onto chitosan/NaOH/fly ash composites: equilibrium, kinetics, thermodynamics and modeling, J. Environ. Chem. Eng., 6 (2018) 1486–1499.

[44] S. Noreen, U. Khalid, S.M. Ibrahim, T. Javed, A. Ghani, S. Naz, M. Iqbal, ZnO, MgO and FeO adsorption efficiencies for direct sky blue dye: equilibrium, kinetics and thermodynamics studies, J. Mater. Res. Technol., 9 (2020) 5881–5893.

[45] L. Sellaoui, F.E. Soetaredjo, S. Ismadji, A. Bonilla-Petriciolet, C. Belver, J. Bedia, A. Ben, A. Erto, Insights on the statistical physics modeling of the adsorption of Cd^{2+} and Pb^{2+} ions on bentonite-chitosan composite in single and binary systems, Chem. Eng. J., 354 (2018) 569–576.

[46] H. Jiang, Y. Dai, Vitamin C modified crayfish shells biochar efficiently remove tetracycline from water: a good medicine for water restoration, Chemosphere, 311 (2023) 136884, doi: 10.1016/j.chemosphere.2022.136884.

[47] L. Sellaoui, F.E. Soetaredjo, S. Ismadji, E.C. Lima, G.L. Dotto, A. Ben, A. Erto, New insights into single-compound and binary adsorption of copper and lead ions on a treated sea mango shell: experimental and theoretical studies, Phys. Chem. Chem. Phys., 19 (2017) 25927–25937.

[48] X. Liu, Z. Shao, Y. Wang, Y. Liu, S. Wang, F. Gao, Y. Dai, New use for *Lentinus edodes* bran biochar for tetracycline removal, Environ. Res., 216 (2023) 114651, doi: 10.1016/j.envres.2022.114651.

[49] J.W. Fu, Q.Q. Xin, X.C. Wu, Z.H. Chen, Y. Yan, S.J. Liu, M.H. Wang, Q. Xu, Selective adsorption and separation of organic dyes from aqueous solution on polydopamine microspheres, J. Colloid Interface Sci., 461 (2016) 292–304.

[50] Y. Dai, Y. Liu, Y. Wang, W. Fang, Y. Chen, Y. Sui, A practice of conservation tillage in the Mollisol region in Heilongjiang Province of China: a mini review, Pol. J. Environ. Stud., 32 (2023) 1479–1489.

[51] W.H. Zou, H.J. Bai, S.P. Gao, Competitive adsorption of neutral red and Cu^{2+} onto pyrolytic char: isotherm and kinetic study, J. Chem. Eng. Data, 57 (2012) 2792–2801.

[52] L. Liu, X. Li, X. Wang, Y. Wang, Z. Shao, X. Liu, D. Shan, Z. Liu, Y.J. Dai, Metolachlor adsorption using walnut shell biochar modified by soil minerals, Environ. Pollut., 308 (2022) 119610, doi: 10.1016/j.envpol.2022.119610.

[53] A. Mittal, J. Mittal, A. Malviya, D. Kaur, V.K. Gupta, Adsorption of hazardous dye crystal violet from wastewater by waste materials, J. Colloid Interface Sci., 343 (2010) 463–473.

[54] L. Liu, Y. Dai, Strong adsorption of metolachlor by biochar prepared from walnut shells in water, Environ. Sci. Pollut. Res., 28 (2021) 48379–48391.

[55] S. Singh, A.G. Anil, S. Khasnabis, V. Kumar, B. Nath, V. Adiga, T.S.S.K. Naik, S. Subramanian, V. Kumar, J. Singh, P.C. Ramamurthy, Sustainable removal of Cr(VI) using graphene oxide-zinc oxide nanohybrid: adsorption kinetics, isotherms and thermodynamics, Environ. Res., 203 (2022) 111891, doi: 10.1016/j.envres.2021.111891.

[56] L. Liu, X. Wang, W. Fang, X. Li, D. Shan, Y. Dai, Adsorption of metolachlor by a novel magnetic illite–biochar and recovery from soil, Environ. Res., 204 (2022) 111919, doi: 10.1016/j.envres.2021.111919.

[57] H. Hosseinzadeh, S. Mohammadi, Quince seed mucilage magnetic nanocomposites as novel bioadsorbents for efficient removal of cationic dyes from aqueous solutions, Carbohydr. Polym., 134 (2015) 213–221.

[58] Y. Dai, J. Shi, N. Zhang, Z. Pan, C. Xing, X. Chen, Current research trends on microplastics pollution and impacts on agro-ecosystems: a short review, Sep. Sci. Technol., 57 (2022) 656–669.

[59] J. Qu, Z. Li, Z. Wu, F. Bi, S. Wei, M. Dong, Q. Hu, Y. Wang, H.Yu, Y. Zhang, Cyclodextrin-functionalized magnetic alginate microspheres for synchronous removal of lead and bisphenol A from contaminated soil, Chem. Eng. J., 461 (2023) 142079, doi: 10.1016/j.cej.2023.142079.

[60] F. Ullah, G.Z. Ji, M. Irfan, Y. Gao, F. Shafiq, Y. Sun, Q. Ul Ain, A.M. Li, Adsorption performance and mechanism of cationic and anionic dyes by KOH activated biochar derived from medical waste pyrolysis, Environ. Pollut., 314 (2022) 120271, doi: 10.1016/j.envpol.2022.120271.

[61] J. Qu, R. Liu, X. Bi, Z. Li, K. Li, Q. Hu, X. Zhang, G. Zhang, S. Ma, Y. Zhang, Remediation of atrazine contaminated soil by microwave activated persulfate system: performance, mechanism and DFT calculation, J. Cleaner Prod., 399 (2023) 136546, doi: 10.1016/j.jclepro.2023.136546.

[62] Y. Dai, K. Zhang, X. Meng, J. Li, X. Guan, Q. Sun, Y. Sun, W. Wang, M. Lin, M. Liu, S. Yang, Y. Chen, F. Gao, X. Zhang, Z. Liu, New use for spent coffee ground as an adsorbent for tetracycline removal in water, Chemosphere, 215 (2019) 163–172.

[63] J. Qu, F. Bi, Q. Hu, P. Wu, B. Ding, Y. Tao, S. Ma, C. Qian, Y. Zhang, A novel PEI-grafted N-doping magnetic hydrochar for enhanced scavenging of BPA and Cr(VI) from aqueous phase, Environ. Pollut., 321 (2023) 121142, doi: 10.1016/j.envpol.2023.121142.

[64] Z. Liu, S. Cui, Q. Fu, F. Zhang, Z. Zhang, R. Hough, L. An, Y. Li, L. Zhang, Transport of neonicotinoid insectics in a wetland ecosystem: has the cultivation of different crops become the major sources?, J. Environ. Manage., 339 (2023) 117838, doi: 10.1016/j.jenvman.2023.117838.

[65] J. Qu, Y. Yuan, X. Zhang, L. Wang, Y. Tao, Z. Jiang, H. Yu, M. Dong, Y. Zhang, Stabilization of lead and cadmium in soil by sulfur-iron functionalized biochar: performance, mechanisms and microbial community evolution, J. Hazard. Mater., 425 (2022) 127876, doi: 10.1016/j.jhazmat.2021.127876.

[66] U. Kamran, H.N. Bhatti, S. Noreen, M.A. Tahir, S.J. Park, Chemically modified sugarcane bagasse-based biocomposites for efficient removal of acid red 1 dye: kinetics, isotherms, thermodynamics, and desorption studies, Chemosphere, 291 (2022) 132796, doi: 10.1016/j.chemosphere.2021.132796.

[67] Y. Ke, F. Zhang, Z. Zhang, R. Hough, Q. Fu, Y. Li, S. Cui, Effect of combined aging treatment on biochar adsorption and speciation distribution for Cd(II), Sci. Total Environ., 867 (2023) 161593, doi: 10.1016/j.scitotenv.2023.161593.

[68] J. Qu, S. Wei, Y. Liu, X. Zhang, Z. Jiang, Y. Tao, G. Zhang, B. Zhang, L. Wang, Y. Zhang, Effective lead passivation in soil by bone char/CMC-stabilized FeS composite loading with phosphate-solubilizing bacteria, J. Hazard. Mater., 423 (2022) 127043, doi: 10.1016/j.jhazmat.2021.127043.

[69] S. Cui, Y. Ke, Q. Fu, R. Hough, Z. Zhang, Z. Shen, L. An, Y. Li, Optimization preparation of biochar from garden waste and quantitative analysis for Cd^{2+} adsorption mechanism in aqueous solution, Biomass Convers. Biorefin., (2022), doi: 10.1007/s13399-022-03289-0.

[70] H. Luo, S.X. Zhang, X.Y. Li, Q. Xu, J.S. Liu, Z.H. Wang, A facile route for preparation of magnetic biomass activated carbon with high performance for removal of dye pollutants, Environ. Sci. Pollut. Res., 24 (2017) 15599–15608.